Glass-like Cerium containing sol-gel coatings for corrosion protection of aluminium and magnesium alloys

N.C. Rosero-Navarro[1], M. Curioni[2], Y. Castro[1], M. Aparicio[1], G.E.Thompson[2], A. Durán[1]

[1]Instituto de Cerámica y Vidrio (CSIC), Campus de Cantoblanco, 28049 Madrid, Spain

[2] Corrosion and Protection Centre, School of Materials, The University of Manchester, M13 9PL, England, United Kingdom

Abstract

This work reports the preparation of glass-like, environmentally-friendly, cerium-based coatings for active corrosion protection of aluminium and magnesium alloys. It describes the preparation of cerium sol-gel sols from cerium nitrate and their deposition by immersion and automatic spray onto aluminium and magnesium alloys to produce uniform coatings with amorphous structures (Ce_xO_y). The coatings are characterised by profilometry, SEM, Spectral Ellipsometry and UV-visible to analyse the structure and density of the glass-like cerium coatings as well as their redox ratio Ce^{4+}/Ce^{3+} as a function of sintering temperature. Finally, electrochemical measurements (EIS) and standard corrosion tests (neutral salt spray, filiform corrosion test, immersion emission test and adhesion on embossing and T-bend test) are performed to study the corrosion behaviour of the cerium glass-like coatings on aluminium and magnesium alloys. EIS measurements confirm the healing or blocking of the defects by the corrosion inhibition species. Excellent corrosion protection behaviour is provided by cerium glass-like coatings, satisfying the most restringing industrial requirements.

1. Introduction

Through alloying and appropriate heat treatment, aluminium alloys of high strength to weight ratio and damage tolerance are available for widespread applications in aircraft

and automobile designs. With appropriate corrosion control systems, corrosion susceptibility of aluminium alloys is acceptable under service conditions. With further demands on light- weighting to reduce fuel consumption and emissions, magnesium alloys, with a density two-thirds that of aluminium [1], are attractive for the transport sector [2]. Additionally, magnesium alloys benefit from high thermal conductivity, dimensional stability, electromagnetic shielding behaviour, and good machinability, together with easy recycling. However, the poor corrosion resistance severely limits extensive applications in a variety of sectors.

A promising strategy to improve the corrosion resistance of magnesium alloys is the application of active conversion coatings, usually obtained from corrosion inhibitor-containing baths. These treatments offer self-healing protection, defined as the ability of a material to recover/repair damage automatically, without external intervention.

Generally, chromate conversion coatings represent the state-of-the-art for industrial applications [3,4], with their high efficiency/cost ratio making them the benchmark for corrosion inhibition. Two types of chromate-based coatings have been widely used, namely chromate conversion coatings (CCC) in the thickness range of 300-500 nm, and chromic acid anodizing (CAA) to generate porous anodic films of several microns thickness. The protection systems usually include chemical or electrochemical pre-treatment, followed by application of epoxy primers and polymeric top-coats [5,6].

In spite of their excellent corrosion protection behaviour, chromates are now declared environmentally hostile, since they are carcinogenic, produce DNA damage, skin allergy, asthmatic reactions, and ulcerations [7]. Consequently, the European

Community has forbidden the use of chromate coatings in all industrial sectors, except aeronautics, from July 2007[8]. Thus, replacing chromium-based coatings by environmentally-friendly systems has triggered the study and development of protective systems containing alternative corrosion inhibitors. In particular, cerium and other rare earth elements have shown promise as alternatives to chromium-based systems [9-11]. Hinton et al. [12,13] proposed cerium-based coatings as a potential alternative to chromate coatings, reporting that precipitation of cerium oxide, cerium hydroxides or cerium hydrates on cathodic sites improved the corrosion resistance. Although the protection mechanism is not totally understood, the corrosion inhibition role of cerium has been confirmed by different electrochemical techniques, including EIS [14,15], split cell technique, and image assisted electrochemical noise analysis [16].

Different non-chromate conversion coatings (NCCC) are obtained from aqueous solutions of rare earths with or without the presence of activator agents [17], phosphate conversion coatings or coatings obtained by deposition of conducting polymers. Films produced from fluorotitanic or fluorozirconic acids, cobalt salts, and phosphate permanganate coatings are available, but they are less effective than the previous traditional chromate treatments [18-21].

Sol–gel technology is an alternative approach for coating generation, being environmentally- compliant and compatible with organic paints. A key advantage of sol-gel films as conversion coatings resides in their covalent bonding and strong adhesion to the substrate, as well as the barrier effect, limiting transport of water to the alloy surface [22,23]. Inorganic sol–gel coatings offer excellent barrier properties [24,25], but the high temperatures required for coatings densification are usually

incompatible with the preservation of light alloys microstructure and properties. In order to remedy the previous, organic and hybrid coatings containing cerium, vanadium, molybdenum, lanthanides or organic inhibitors have been developed [26-34]. These coatings can be densified at low temperatures without interfering with the tailored microstructure of magnesium alloys. Alkylalkoxides and methacrylate or epoxy-functionalised groups have been used as a base to form barrier-type coatings; the addition of selected inhibitors to the base formulation has also provided self-healing ability [28,30,31]. However, the addition of active species to the precursor sols frequently results in degradation of the barrier properties of the coatings and deactivation of the corrosion inhibitors [35,36]; thereby limiting the industrial requirements.

For active inhibition, pure cerium oxide coatings have been prepared from aqueous sol-gel suspensions [37], with many containing CeO_2 nano-particles. With sintering at relatively high temperatures of 350-800ºC, the resultant coatings were crystalline. [38-43].

The aim of this work is to establish a new procedure for producing glass-like, environmentally-friendly, cerium-based coatings for active corrosion protection of aluminium and magnesium alloys. The coatings, generated from alcoholic sol-gel sols, are densified at reduced sintering temperatures, i.e. below 250ºC. This method [44] produces uniform coatings with amorphous structures excellent adhesion to the metallic substrates and to various organic primers. The process involves the stabilisation of Ce^{3+} ions in a glass-like structure, a primary route to facilitate their diffusion or migration to damaged regions to inhibit localised corrosion. The coatings present active self-healing

behaviour, hindering corrosion activity at defects, as confirmed by electrochemical techniques. Further, the Ce_xO_y glass-like coatings can be used in conjunction with paint systems, primers and/or topcoats, to provide further corrosion resistance. Aluminium and magnesium alloys treated with the cerium-based coatings successfully passed various, commonly accepted, accelerated corrosion tests. Thus, the treated substrates pass the most stringent requirements of the aircraft, automobile and building industries, thereby providing a suitable alternative to chromium-based coatings and may be a new benchmark for self-healing protecting coatings.

2. Experimental

Preparation and characterisation of Cerium sol-gel sols. Cerium sol-gel sols were prepared with pH=2 (labelled as Ce-Al sol) and pH= 6 (labelled as Ce-Mg sol) employing cerium nitrate $Ce(NO_3)_3.6H_2O$ as precursor. For both sols the preparation involved two steps. In the common first step, a cerium nitrate solution was prepared dissolving 39,1g of cerium nitrate in 142 g of ethanol and 13,8 g of acetic acid. In the second step of Ce-Al sol, 8,5 g of citric acid and 6,5 g of butanediol were added to the cerium nitrate solution resulting in a final pH close to 2. In the case of Ce-Mg sol, 2,85 g diethanolamine and 3 g glycidyl-methacrylate were dissolved in the initial cerium nitrate sol leading to a pH sol close to 6. Both sols were stored at 5ºC; their stability was evaluated by following the viscosity evolution with time using a rheometer (Haake RS50, Germany). The synthesis of both sols was scaled-up to pilot plant scale, 5 L, for deposition with industrial spraying robots.

Metal Substrate preparation. Aluminium alloy AA2024 was exposed to a three-step cleaning procedure with a surface preparation including an alkaline cleaning (Metaclean T2001 – Chemie Vertrieb Hannover GmbH & Co KG), an alkaline etching (Turco

Liquid Aluminetch Nr.2 – Turco Chemie GmbH) and a following step of acid etching (Turco Liquid Smutgo NC – Turco Chemie GmbH). The aluminum alloy AA3105 was cleaned using alkaline etching (Gardoclean S 5080 – Chemetall) and acid desmutting (Gardoclean 450 – Chemetall) at 45ºC.

Magnesium alloy MgAZ-31 was pre-treated by mechanical polishing using an emery paper up to #2000 and then cleaned with nitric acid (0.01N), for 30 seconds. The MgAZ91 alloy was exposed to two-step cleaning procedure, first with NaOH 2,5 N for 5 min and subsequent 10 min in HF 10 vol%.

Deposition methods and treatments of cerium coatings. Ce-Al sol-gel sol was applied onto AA2024 and AA3105 substrates by automatic spray. The coatings were densified during 12 hours at 120 ºC in air. A complete protection system was obtained on AA2024 by automatic spray at Fraunhofer Institut Produktiontechnik und Automatisierung (IPA, Germany) using an epoxy primer of 15-25 μm and a top-coat of 20-30 μm (Mankiewicz) deposited onto the Ce-Al glass-like coatings (labelled as AA2024-complete Ce-Al system). In the case of AA3105 alloy, Ce-Al glass-like coatings were covered by a polyester based paint (primer CP22-0422 White Basf, and top-coat CI24-0095 P S White) applied by coil coating at PLALAM (labelled as AA3105-complete Ce-Al system).

Ce-Mg sol-gel sol was deposited on MgAZ91 and MgAZ-31 substrates by dip-coating at a withdrawal rate of 30 cm/min and densified during 10 min at 250 ºC in air. A primer coat of 15-20 μm was further applied by automatic spray over Ce-Mg glass-like coating on MgAZ-91 alloy to get a complete protection system (MgAZ91-complete Ce-Mg system).

Physical and Electrochemical characterisation of coatings. The coating thickness was measured by profilometry (Talystep-Taylor Hobson, UK) and SEM (ZEISS EVO 50). A Spectroscopic ellipsometer (Woollam M2000U, USA) was utilised to determine the coating thickness and refraction index and their change with room humidity.

Coatings produced from both sols were analysed by Grazing X-ray diffraction (GXRD using CuKα radiation in a Panalytical diffractometer (X'Pert PRO theta/theta) in order to analyse the possible crystallisation of CeO_2 on the films deposited on glass substrates. The diffraction patterns were recorded in the range of $2\theta = 20–70$ º, using a fixed counting time of 20 s/step and an increment of 0.05º.

Ultraviolet-visible spectra (Perkin Elmer, Lambda 950) were recorded in transmission mode for coatings deposited on SiO_2 substrates. Ce^{3+}/Ce^{4+} ratio was determined in both types of films after deconvolution of absorption curves using Origin 8.

Electrochemical impedance spectroscopy was performed on MgAZ-31, bare and protected with the Ce-Mg glass-like coating as a function of the immersion time in 0.35 gL^{-1} NaCl aqueous solution. EIS measurements were performed using a Solartron Modulab potentiostat at open circuit potential with AC voltage amplitude of 10 mV with respect to a saturated calomel electrode (SCE), in the frequency range from 10 mHz to 40 kHz. The area exposed (working electrode area) to the electrolyte was 7.5 cm^2 and platinum sheet was used as counter electrode.

Standard corrosion tests. The AA2024-complete Ce-Al system was scratched and exposed to neutral salt spray test (SST) following ASTM B-117. For inspection, samples were washed with deionized water, dried and examined at intermediate times up to 1000 hours. Filiform corrosion test (EN 3665) was also performed on this system according to U-type scratch. After initiation with concentrated hydrochloric acid the

samples were placed in the test chamber at an angle of 6° from the vertical, and evaluated by visual inspection at 168, 500 and 960 hours. Immersion- emersion test was also applied to this system (DIN-EN-3212).

AA3105 alloy protected with the AA3105 complete Ce-Al system was tested with Adhesion on embossing and T-bend tests according with ISO 6272-2-2006 and ECCA T7 -1996, respectively.

MgAZ91-complete Ce-Mg system was tested by scribing (adhesion test) and scratching combined with neutral salt spray test up to 312 hours following ASTM-117 and Adhesion complemented with SST.

3. Results and Discussion

3.1. Characterisation of the sols and deposition of the coatings

Cerium sol-gel sols with acid (Ce-Al sol) and neutral (Ce-Mg sol) pH were prepared following the processes described in the experimental part. Cerium nitrate $Ce(NO_3)_3.6H_2O$ was mixed with solvents and complexing agents in selected molar ratios to improve the stability of the sols and to control their final pH. Glacial acetic acid, citric acid and diethanolamine were selected as complexing agents.

The final pH of the sol is a key parameter to prevent the degradation of the substrates and the associated loss of chemical and mechanical properties, and corrosion resistance. The optimum pH is 2 for aluminium alloys, and in the range of 6-7 for magnesium alloys. The initial pH of the Ce-Al sol was 2, increasing to 6-7 with addition of diethanolamine (Ce-Mg sol). The presence of one or more organic solvents, ethanol and/or butanediol, supplied the desired adherence to the substrate as well as aiding dissolution of the salts and complexing agents. Both sols show Newtonian behaviour

with a viscosity around 2 mPa. The stability of the individual Ce-Al and Ce-Mg sols was improved by storing at 5°C, with the properties unchanged for more than 90 days.

Prior to deposition of the Ce-Al and Ce-Mg sols, the alloy substrates underwent a surface modification process and/or cleaning process. The procedures used for AA2024, AA3105 and MgAZ91 alloys were alkaline cleaning/ alkaline etching/acid etching, alkaline etching/acid dismutting, and alkaline /acid process respectively. Mechanical polishing and cleaning with acid solutions were used for the MgAZ31 alloy.

After alloy pre-treatment, cerium glass-like coatings were deposited by immersion or automatic spraying. The Ce-Al sol was used for coating AA2024 and AA3105 substrates with a robot automatic spray, whereas the MgAZ91 and MgAZ31 alloys were coated by immersion in the Ce-Mg sol using a withdrawal rate of 30 cm/min. Transparent and uniform Ce_xO_y glass-like coatings were obtained after drying and thermal treatment at 120ºC for 12 hours for the aluminium alloys (Ce-Al coats), and treatment at 250ºC for 10 min for the magnesium alloys (Ce-Mg coats). All the coatings, with thickness around 600 nm, were highly adherent, yellow-coloured and totally transparent after the thermal treatment. The amorphous structure and the absence of crystallisation or precipitated phases were confirmed by unreported XRD analysis.

SEM observation revealed that the coatings covered the macroscopic alloy surface; although the films are cracked, neither peeling nor flaking of the coatings was evident. Since the main function of the coatings is to provide active corrosion protection, the barrier against the environmental access is offered by the paint system applied onto the Ce_xO_y glass-like coatings. Thus, complete protection systems were produced using

AA2024 and AA3105 alloys by combining the Ce-Al film with a primer and a topcoat, using automatic spray in both cases (AA2024 and AA3105 complete Ce-Al systems). A single primer coat was used as finishing process for the Ce-Mg glass-like coatings on MgAZ91 (MgAZ91 complete Ce-Mg system).

3.2. Optical characterization of the coatings

There is abundant literature on crystalline CeO_2 coatings, due to the interesting properties of high refractive index, high transparency in the visible, near and middle-IR, strong adhesion, and high stability against mechanical abrasion, chemical attack and high temperature [45,46].

The structure and density of the coatings depends largely on the deposition technique. Oxide films deposited by vacuum evaporation generally display a columnar structure with many pores that are readily filled by moisture under ambient conditions [47].UV-visible spectroscopy, probing the absorption band appearing around 2,97μm, can be used for determining the water content. The transmittance spectra of Ce-Al coatings displayed a pronounced dependence on humidity, with a wide and increasing band around 3 μm indicating high open porosity. A similar, but less pronounced behaviour was observed for the Ce-Mg coatings also suggesting porous morphologies (not shown). Spectral ellipsometry was used to measure the refractive index and thickness of the coatings following exposure to ambient humidity. Thus, the relative film density of both coatings was calculated using relatively dense (3,93 g/cm^3) CeO_2 [48] as a reference. Ce-Al films present a pore volume of 43%, while Ce-Mg coatings, in agreement with

the increased sintering temperature, show a reduced total pore volume of 34%; both values are in good agreement with the literature.

UV-visible spectra were acquired between 190 and 1000 nm on Ce-Al and Ce -Mg coatings, deposited on SiO_2 substrates and treated under similar conditions to the practical alloys, to examine the redox ratio of Ce^{3+}/Ce^{4+}. **Figure 1A** shows the absorption spectra of thin Ce-Al and Ce-Mg coatings on the SiO_2 substrates. Two main bands appear in both spectra; one band is centred on 200 nm and assigned to Ce^{4+} charge transfer, with a further, wider band around 265 nm in Ce-Al films and shifted to near 310 nm in Ce-Mg coats, associated with Ce^{3+}.

Deconvolution of the Ce-Al spectra confirmed the qualitative analysis, with two bands centred at 201 nm and 267 nm. Conversely, deconvolution of the Ce-Mg spectra resulted in three bands at 198, 265 and 310 nm (**Figure 1B**). Calculation of the redox ratio Ce^{4+}/Ce^{3+} requires knowledge of the molar absorptivity (ε) corresponding to the different transitions observed. ε can be derived from the absorption coefficient α, (Equation 1) and the extinction coefficient *k*, (equation 2) using the expressions:

$$\alpha = 4\pi k / \lambda \quad (1)$$

$$\varepsilon = 4\pi k / \lambda C \quad (2)$$

where λ is the wavelength of the incident light and C is the ion concentration.

Ce^{4+} is a $4f^0$ system, with no f→f transitions; the colour of Ce^{4+} salts arises from the tail of a strong charge transfer band in the UV, around 200 nm independently of the environment, from glass matrices to pure CeO_2 films. Although the wavelength of this electronic transition is nearly constant, the molar absorptivity changes significantly, depending on the nature of the complex and on the electronegativity of the ligands [49],

varying from 3800 $L.mol^{-1}.cm^{-1}$ in silicate glasses up to 4000- 7000 $L.mol^{-1}.cm^{-1}$ in crystalline CeO_2 films deposited by different techniques and with different nanostructures [45].

Ce^{3+} has a $4f^1$ ground electronic configuration with two free ions states separated by about 2000 cm^{-1}. The first excited configuration is 5d and the optical spectra of Ce^{3+} therefore consist on one f→f transition in the near IR that is Laporte forbidden with very low molar absorptivity, and two f→d transitions ($^2F_{5/2} \rightarrow {}^2D_{3/2,\ 5/2}$) Laporte allowed nf → n-1fd transitions in the UV [50]. The band maxima corresponding to these transitions depend mainly on the neighbouring ligands, being situated at 262, 298 and 328 in ethanol solvent. Since cerium glass-like coatings are prepared from alcohol sols, and the UV-visible absorption bands appear at similar wavelengths (267 and 310 nm), it is reasonable to assign the molar absorptivities corresponding to these bands, 480 and 150 $L.mol^{-1}.cm^{-1}$ for a semi-quantitative calculation of Ce^{3+} concentration. The band at 328 nm is not visible because ε is very low.

From the data, calculated redox ratios for both glass-like cerium coatings are 0.55/0.45 for Ce-Al, and 0.05/0.95 for Ce-Mg, in good agreement with the higher sintering temperature of Ce-Mg films that shifts the redox ratio to reducing conditions.

3.3 Electrochemical and standard corrosion tests

Various experimental techniques can be used to study the anticorrosion performance of the coatings. Accelerated corrosion tests, especially salt spray tests (SST), are valuable for validation and comparison of the performance between different coatings. However, such tests provide little information on the interaction between the inhibitors and the alloys, or the mechanism of protection.

Electrochemical impedance spectroscopy (EIS), on the other hand, is widely used to characterise the corrosion behaviour of coating systems, allowing not only comparison of different systems but also providing relevant information about coating degradation and the corrosion mechanism. Both, EIS and SST were used to assess the performance of the Ce_xO_y glass-like coatings on the aluminium and magnesium alloys.

EIS was used to analyse the corrosion behaviour of Ce-Mg glass-like coatings on MgAZ31 in 0.35 wt % NaCl electrolyte under naturally aerated conditions and room temperature for immersion times up to 200 h (**Figure 2**). The impedance spectrum for the bare MgAZ31 specimen after immersion for 1 and 10 hours are included as reference.

Important differences on the corrosion behaviour can be derived from the spectra. The impedance modulus (/Z/) at 0.01 Hz of the cerium glass-like coated MgAZ31 initially decreases with immersion time to 2 x 10^4 Ωcm^2 after 31 h. This drop is related to the breakdown of the film and corrosion activity commencing on the bare metal surface. However, after 55 h, /Z/ shows an important increase, surpassing the initial values, and continues to increase to 2 x 10^5 Ω/cm^2 after immersion for 193 h, i.e. two orders of magnitude higher than the initial value for the bare MgAZ31 alloy. Although bare Mg also shows a partial recovery of impedance at low frequency, the metal appears entirely damaged after 10 hours of immersion. This behaviour is associated with the development of corrosion products that slightly improve the barrier effect of the natural oxide layer. In the case of the coated substrates this effect is magnified significantly by cerium ions.

Scrutiny of the phase plot (**Figure 2**) provides additional information. The absence of a time constant at high frequency (above 10^3 Hz), usually ascribed to coatings with barrier functionality, could be related to a high porosity volume and cracks in the Ce_xO_y glass-like coating.

The relaxation process at 1-10 Hz is usually assigned to the capacitance of the intermediate oxide layer present at the metal/coating interface. The increase of capacitance with immersion time indicates an increase of the corrosion resistance of this interlayer, the last barrier for the corrosive species before reaching the alloy surface [50]. After immersion for 4 h, the curve reveals two time constants at 10 and 0.03 Hz, attributed to the response of a mixed Ce_xO_y / magnesium oxide layer and to the charge transfer controlled processes, respectively. The initiation of corrosion activity triggers active corrosion protection provided by cerium species. Increase of the immersion time produces first a decrease (activation step) and then a rise in the phase angle with a shift to lower frequencies, suggesting the precipitation of a dense oxide layer formed by magnesium oxide from corrosion and highly insoluble cerium compounds. The consequence is the observed increase of impedance with immersion time [50].

It is clear that the recovery of the impedance at low frequency (**Figure 2**) and the absence of significant corrosion processes are related to the presence of Ce_xO_y glass-like coating as inhibition agent. The glass-like, porous structure of Ce-Mg coatings, with more than 95% of cerium ions present as Ce^{3+}, allows the fast diffusion of Ce^{3+} to the electrolyte and the subsequent precipitation on the corrosion sites as cerium oxides, hydroxides and even hydrates as a result of local pH change. Although the composition of the precipitates on the defects was not identified, EIS spectra confirm the healing or blocking of the defects by the corrosion inhibition species. The electrochemical

behaviour is thus a clear indication of active self-healing corrosion protection provided by the Ce_xO_y glass-like coatings [47**]**

Standard corrosion tests usually employed in the aeronautic, automotive and other metallurgical industries were also performed to asses the anticorrosion performance of Ce_xO_y glass-like coatings on the different substrates. SST was performed on the AA2024-complete Ce-Al system according to standard ASTM B117. The substrates, provided by EADS, were sections cut from large demonstrator panels. The main focus of the corrosion tests was the investigation of the stringer areas, where the coating thickness was low due to limited accessibility of the spraying process. The deposition of Ce-Al coatings from a scaled-up Ce-Al sol and further protection with primer and top-coat was performed at IPA (Stuttgart) and tested by EADS. The panels were scribed and exposed in a neutral salt spray for times up to 1000 h. The panels were removed at intermediate times, with visual inspection showing no defects on the scratched region. Only minor corrosion occurs in the scribed region, indicating active protection of the coating system (not shown).

The same system was subjected to filiform attack, by scratching according to U-type and maintained in the chamber test up to 960 h. Visual observation at 168, 500 and 960 h (**Figure 3**) showed excellent protection against filiform corrosion. The scratch appears without defects, even on stringers or welding seam, indicating high resistance of the coatings to the propagation of defects.

Alternate immersion- emersion test was also carried out on this system according to DIN EN 3212, revealing protection in the scratched area, and confirming the active protection process.

AA3105 complete Ce-Al system was tested also by evaluating adhesion on a T-bend and after embossing. These tests enable evaluation of the flexibility and adhesion of

coatings by observing the presence of cracks or loss of adhesion in the regions where the coated substrate is bent or deformed. **Figure 4** shows the AA3105-complete Ce-Al system (glass-like Ce-Al coating deposited at IPA and painted at PLALAM by coil coating with polyester based primer and top-coat) a) after adhesion on embossing and b) after T-bend adhesion tests.

The macroscopic image from the embossing test shows that the complete system is capable of resisting the impact without peeling or cracking. Similar behaviour was observed in the case of the T-bend test. The system was bent through 2º without flaking or peeling. Adhesion tests reveal the excellent resistance to impact and cracking of the AA3105-complete Ce-Al system. Corrosion penetration and adhesion after 1000 h of neutral salt spray (SST) also showed outstanding results satisfying the most restringing industrial requirements.

MgAZ91-complete Ce-Mg system was also exposed to neutral salt spray (SST) and adhesion tests. **Figure 5A** and **B** displays the surface appearance of protected samples after 24 and 312 h in SST respectively. After coating and before testing, a hole was drilled in the bottom region of the samples, where the MgAZ91 substrates were only coated by the primer. A dotted line indicates the level of the cerium glass-like coating, this enabling comparison of the corrosion behaviour of the substrate with and without cerium glass-like coating.. Visual inspection of the scribed region after removal from the SST chamber shows minor deterioration of the complete protection system, indicating good adhesion and active protection. The outcome of the adhesion test for system on MgAZ91 is presented in **Figure 5C** and **D.** Visual observation shows that the scratched regions are perfectly adhered and no peeling or material loss is revealed. Some delamination or chipping was detected at the edges of the samples, where the lack of Ce-Mg coating may have been introduced due to sample geometry. The zone

surrounding the hole exhibits significant corrosion that propagates to some extent. This confirms that the presence of Ce-Mg glass-like coating reduces significantly the metal susceptibility to corrosion.

4. Conclusions

Uniform Ce_xO_y glass-like coatings can be produced by immersion or automatic spray with subsequent sintering temperatures from 120ºC up to 250°C that are sufficiently low to avoid deterioration of the alloy microstructure and mechanical performance. Electrochemical and standard corrosion tests demonstrate that cerium glass-like coatings display outstanding anticorrosion properties on various substrates. The experimental results confirm that active corrosion protection (self healing) is provided by cerium coatings on by blocking or healing of the defects through the inhibition capability of cerium products. The SST and adhesion tests results show that cerium-based systems are a suitable alternative to chromium-based systems, providing a new benchmark for self-healing protective coatings.

Acknowledgements

Authors acknowledge the funding provided by the European Community, MULTIPROTECT project: "Advanced environmentally friendly multifunctional corrosion protection by nanotechnology", Contract Nº NMP3-CT-2005-011783 and especially to EADS Innovation Works, PLALAM.SpA and INASMET-Tecnalia.

Reference

[1] L. B.. Duffy, Mater World (UK), 4 (1996) 127.

[2] J.E. Gray, B. Luan J. Alloys Compd, 336 (2002) 88.

[3] T. L. Metroke, R. L. Parkhill, E. T. Knobbe Prog Org Coat, 41 (2001) 233.

[4] P. Campestrini, E. P. M. Van Westing, A. Hovestad, J. H.W. de Wit Electrochem. Acta, 47 (2002) 1098.

[5] M. Bethencourt, F. J. Botana, J. J. Calvino, M. Marcos, M. A. Rodriguez-Chacon, Corros Sci, 11 (1998) 1803.

[6] J. H. Osborn, Prog Org Coat, 41 (2001) 280.

[7] A. Caglieri, M. Goldoni, O. Acampa, R. Antreoli, M.V. Vettori, M. Corradi, P. Apostoli, A Mutti Environ Health Perspect, 114 (2006) 542

[8] U.S. Public Health Service, Report no. STSDR/TP-88/10 July, 1989.

[9] A. E. Hughes, R. J. Taylor, B. R. W. Hinton, L. Wilson, Surf Interface Anal, 23 (1995) 540.

[10] V. Moutarlier, B. Neveu, M. P. Gigandet, Surf Coat Technol., 202 (2008) 2052.

[11] A. Frutos, M. A. Arenas, Y. Liu, P. Skeldon, G. E. Thompson, J.J. Damborenea, A. Conde**,** Surf Coat Technol, 202 (2008) 3797.

[12] B. R. W. Hinton, D. R. Arnott, N. E. Ryan Mater Forum, 9 (1986) 162.

[13] B. R. W. Hinton, J Alloys Compd, 180 (1992) 15.

[14] M. Zheludkevich, G. Shchukin, K. A. Yasakau, H. Möhwald, M. G. S. Ferreira Chem Mater, 19 (2007) 402.

[15] D. Ho, N. Brack, J.C. Scully, T. Markley, M. Forsyth, B. Hinton J Electrochem Soc, 153 (2006) B392.

[16] NC. Rosero-Navarro, M. Curioni, R. Bingham, A. Durán, M. Aparicio, R. Cottis, G. E. Thompson Corros. Sci, 2010 (sent)

[17] C. Dong-Chu, L. Wen-Fang, G. Wei-Hui, W. Gui-xiang, W. Jian-Feng *Trans* Nonferrous Met Soc China, 19 (2009) 592.

[18] H Wang, C. S. Liu, F. J. Shang Acta Metal, 21 (2008) 269.

[19] S. V. Oleinik, Y. I. Kuznetsov, Protection of Metals, 43 (2007) 391.

[20] S. Wang, C. Liu, F. Shan, Acta Metal, 22 (2009) 161.

[21] M. L. Sienkowski, United States of America Patent 1999, US5885373.

[22] A. Durán, Y. Castro, M. Aparicio, A. Conde, J. J. de Damborenea Int Matert Rev, 52 (2007) 175.

[23] N.C. Rosero-Navarro, SA. Pellice, A. Durán, M. Aparicio Corros Sci, 50 (2008) 1283.

[24] A. Durán, Y. Castro, A. Conde, J.J. de Damborenea, Handbook on Sol-gel Technology. Vol.3. Chapter 19 Edited by Sumio Sakka. Kluwer Academic Publishers. (2004) 399.

[25] Y. Castro, A. Duran, R.Moreno, B. Ferrari Adv Mater, 14 (2002) 505.

[26] M. Zaharescu, L. Predoana, A. Barau, D. Raps, F. Gammel, N. C. Rosero-Navarro, Y. Castro, A. Durán, M. Aparicio Corros Sci, 51 (2009) 1998.

[27] Y. Castro, A. Duran, A. Conde, J.J. Damborenea Electrochim Acta, 53 (2008) 6008.

[28] NC. Rosero-Navarro, SA. Pellice, A. Durán, S. Ceré, M. Aparicio J Sol-Gel Sci Technol, 52 (2009) 31.

[29] D. Wang, G.P. Bierwagen Prog Org Coat, 64 (2009) 327.

[30] M. L. Zheludkevich, I. M. Salvado, M.G.S Ferreira, J Mater Chem, 15 (2005) 5099.

[31] N.C. Rosero-Navarro, L. Paussa, F. Andreatta, Y. Castro, A. Durán, M. Aparicio, L. Fedrizzi Surf Interface Anal, 42 (2010) 299.

[32] D. Raps, T. Hack, J. Wehr, M. L. Zheludkevich, A. C. Bastos, M. G. S. Ferreira, O. Nuyken, Corros. Sci, 51 (2009) 1012.

[33] K. A. Yasakau, M. L. Zheludkevich, O. V. Karavai, M. G. S. Ferreira Prog Org Coat, 63 (2008) 352.

[34] M. L. Zheludkevich, K. A. Yasakau, S. K. Poznyak, M. G. S. Ferreira Corro Sci, (2005) 3368.

[35] A. S. Hamdy Mater Lett, 60 (2006) 2633

[36] M. García-Heras, A. Jiménez-Morales, B. Casal, J.C. Galván, S. Radzki, M.A. Villegas J Alloys Compd, 380 (2004) 219

[37] D.G. Shchukin, M.L. Zheludkevich, K.A. Yasakau, S.V. Lamaka, H. Möhwald, M.G.S. Ferreira Adv Mater, 18 (2006) 1672.

[38] H. Hasannejad. M. Aliofkhazraei, A. Shanaghi, T. Shahrabi, A. R. Sabour Thin Solid Films, 517 (2009) 4792.

[39] R.G.Biswas, R. D. Sanders J Mater Eng Perform, 7 (1998) 727.

[40] V.A.C. Haanappel, T. Fransen, B. Geerdink, P. J. Gellings, M. F. Stroosnijder Oxid Met, 35 (1991) 405.

[41] F.Czerwinski, J. A. Szpunar J Sol-Gel Sci Tench, 9 (1997) 103.

[42] R. Haugsrud Corros Sci, 44 (2002) 1569.

[43] N.C. Rosero-Navarro, Y. Castro, M. Aparicio, A. Durán Spanish Paten, P200930982, (2009)

[44] R. G. Toro, G. Malandrino, I. L. Fragala J Phys Chem B, 108 *(*2004) 16357.

[45] S.Debnath, M.R.Islam, M.S.R.Khan Bull Mater Sci, 30 (2007) 315.

[46] G. Atanassov, R. Thielsch, D. Popov Thin Solid Films, 223 (1993) 288.

[47] T. Suzuki, I. Kosacki, V. Petrovsky, H. U. Anderson J Appl Phys, 91 (2002) 2308.

[48] A. Paul, M. Mulholland, M. S. Zaman J Mater Sci, 11 (1976) 2082.

[49] S.V. Lamaka, G. Knörnschild, D.V. Snihirova, M.G. Taryba, M.L. Zheludkevich, M.G.S. Ferreira Electrochi. Act, 55 (2009)131.

[50] M.L. Zheludkevich, K.A. Yasakau, A.C. Bastos, O.V. Karavai, M.G.S. Ferreira Electroche. Commun, 9 (2007) 2622.

5. Figure(s)

Click here to download 5. Figure(s): Roreso-Surf-Fig.doc

Figure 1. (a) Absorption UV-vis spectra of Ce-Al and Ce-Mg glass-like coatings deposited on SiO_2 substrates. (b) Deconvolution of Ce-Mg glass-like spectra to determine the redox Ce^{4+}/Ce^{3+} ratio.

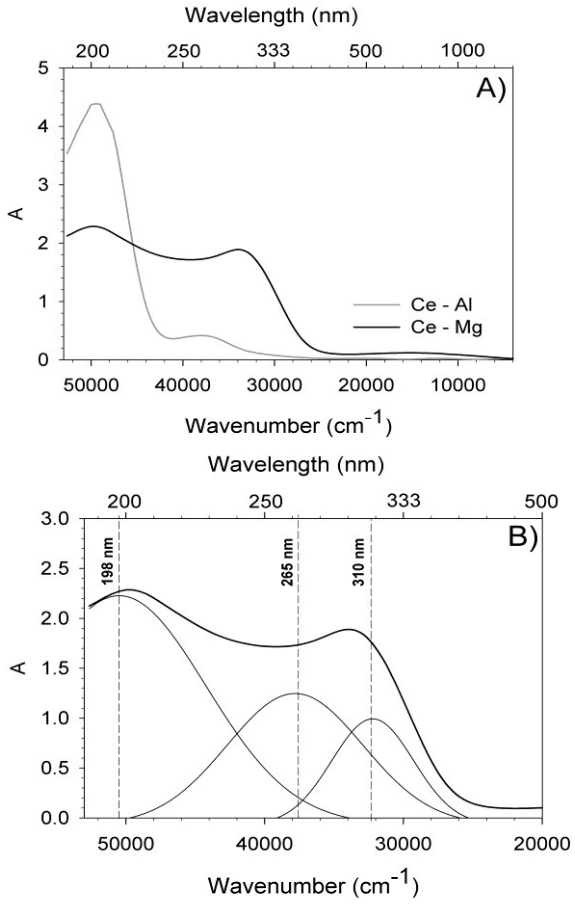

Figure 2. Bode modulus and angle phase plots for Ce_xO_y glass-like coating on MgAZ31 as a function of immersion time in 0.35 wt% NaCl, compared with bare MgAZ31.

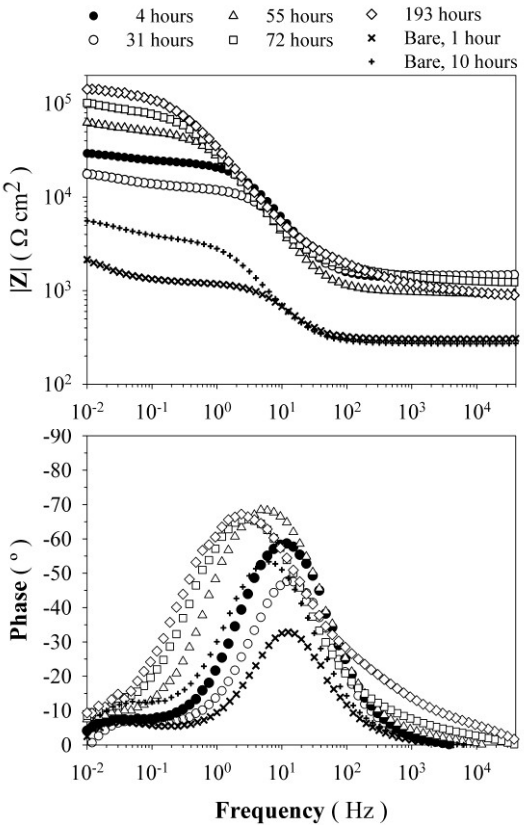

Figure 3. Macrograph of AA2024 complete-Ce-Al system after 960 h of filiform corrosion test.

Figure 4. AA3105 complete Ce-Al system (a) adhesion on embossing and (b) adhesion on T-bend tests.

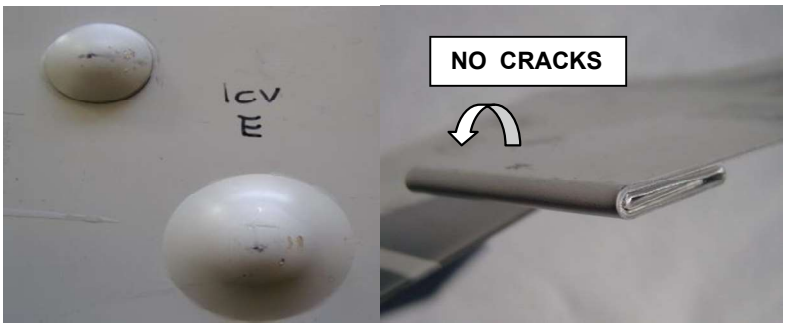

Figure 5. Photographs of the MgAZ91 complete-Ce-Mg system in SST after (a) 24 h and (b) 312 h, and Adhesion test on the same system (c) as prepared and (d) after 312 hours.